NASA/TM—2015-218932

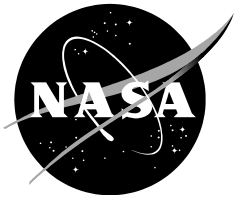

Utilizing Direct Numerical Simulations of Transition and Turbulence in Design Optimization

Man M. Rai
Ames Research Center
Moffett Field, CA-94035

December 2015

NASA STI Program ... in Profile

Since its founding, NASA has been dedicated to the advancement of aeronautics and space science. The NASA scientific and technical information (STI) program plays a key part in helping NASA maintain this important role.

The NASA STI program operates under the auspices of the Agency Chief Information Officer. It collects, organizes, provides for archiving, and disseminates NASA's STI. The NASA STI program provides access to the NTRS Registered and its public interface, the NASA Technical Reports Server, thus providing one of the largest collections of aeronautical and space science STI in the world. Results are published in both non-NASA channels and by NASA in the NASA STI Report Series, which includes the following report types:

- TECHNICAL PUBLICATION. Reports of completed research or a major significant phase of research that present the results of NASA Programs and include extensive data or theoretical analysis. Includes compilations of significant scientific and technical data and information deemed to be of continuing reference value. NASA counterpart of peer-reviewed formal professional papers but has less stringent limitations on manuscript length and extent of graphic presentations.

- TECHNICAL MEMORANDUM. Scientific and technical findings that are preliminary or of specialized interest, e.g., quick release reports, working papers, and bibliographies that contain minimal annotation. Does not contain extensive analysis.

- CONTRACTOR REPORT. Scientific and technical findings by NASA-sponsored contractors and grantees.

- CONFERENCE PUBLICATION. Collected papers from scientific and technical conferences, symposia, seminars, or other meetings sponsored or co-sponsored by NASA.

- SPECIAL PUBLICATION. Scientific, technical, or historical information from NASA programs, projects, and missions, often concerned with subjects having substantial public interest.

- TECHNICAL TRANSLATION. English-language translations of foreign scientific and technical material pertinent to NASA's mission.

Specialized services also include organizing and publishing research results, distributing specialized research announcements and feeds, providing information desk and personal search support, and enabling data exchange services.

For more information about the NASA STI program, see the following:

- Access the NASA STI program home page at http://www.sti.nasa.gov

- E-mail your question to help@sti.nasa.gov

- Phone the NASA STI Information Desk at 757-864-9658

- Write to:
  NASA STI Information Desk
  Mail Stop 148
  NASA Langley Research Center
  Hampton, VA 23681-2199

NASA/TM-2015-218932

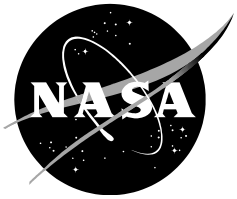

Utilizing Direct Numerical Simulations of Transition and Turbulence in Design Optimization

Man M. Rai
Ames Research Center
Moffett Field, California

National Aeronautics and
Space Administration

Ames Research Center
Moffett Field, California 94035-1000

December 2015

UTILIZING DIRECT NUMERICAL SIMULATIONS OF TRANSITION AND TURBULENCE IN DESIGN OPTIMIZATION

Man Mohan Rai
Ames Research Center

SUMMARY

Design optimization methods that use the Reynolds-averaged Navier-Stokes equations with the associated turbulence and transition models, or other model-based forms of the governing equations, may result in aerodynamic designs with actual performance levels that are noticeably different from the expected values because of the complexity of modeling turbulence/transition accurately in certain flows. Flow phenomena such as wake-blade interaction and trailing edge vortex shedding in turbines and compressors (examples of such flows) may require a computational approach that is free of transition/turbulence models, such as direct numerical simulations (DNS), for the underlying physics to be computed accurately. Here we explore the possibility of utilizing DNS data in designing a turbine blade section. The ultimate objective is to substantially reduce differences between predicted performance metrics and those obtained in reality. The redesign of a typical low-pressure turbine blade section with the goal of reducing total pressure loss in the row is provided as an example. The basic ideas presented here are of course just as applicable elsewhere in aerodynamic shape optimization as long as the computational costs are not excessive.

INTRODUCTION

Computational fluid dynamics (CFD) analyses of propulsion related flows are used in both assessing designs and in formal design optimization efforts to compute performance metrics for any given geometric configuration. These analyses are currently performed with the Reynolds-averaged Navier-Stokes (RANS) equations. On occasion large-eddy simulations (LES) are performed to more accurately compute the underlying physics. Turbulence models are required in both these approaches. These “model-based” computational techniques yield approximations to the true flow physics. Direct numerical simulations (DNS) of turbulent/transitional flows capture all the essential scales of such flows but require grids that provide accurate resolution of the smaller scales (typically about 15 to 25 times as large as the Kolmogorov length scale in turbulent flow) while simultaneously encompassing the entire computational region. In high-Reynolds number flows the smaller scales are significantly smaller than the largest scales and the computational region. This disparity in scales necessitates large grids and consequently, large computational resources. To date, for the most part, DNS has been applied to relatively simple geometries and flows with low to moderate Reynolds numbers.

There are many phenomena in propulsion related flows that may require DNS in order to truly capture the underlying physics. Wake-blade interaction and vortex shedding at trailing edges of blades in rotating machinery are two examples of flow features whose accurate computation may require an approach that does not rely turbulence/transition modeling. These

flow features contribute significantly to the acoustics, unsteady heat transfer, performance losses and dynamic loads on the machine and can thus may have a significant effect on efficiency, reliability, safety and maintenance costs. Here we illustrate this point using a past example involving the Space Shuttle Main Engine (SSME). The system under consideration was an axial turbine with liquid oxygen as the working fluid, the Low Pressure Oxidizer Turbo-Pump (LPOTP). Inspection of the first row of vanes in this turbine showed evidence of high cycle fatigue (HCF) at the trailing edge near the end-walls. CFD analysis of the known sources of HCF indicated vortex shedding as the most probable cause[1]. It was found that the shedding frequency range overlapped the vane trailing edge flapping mode natural frequency. At the time, vanes in the first row of the LPOTP were replaced at carefully monitored time intervals thus ensuring the safety of the Shuttle flights[1]. A first attempt at redesigning the vane is reported in Ref. 1. The objectives pursued were increased vane strength, decreased shedding amplitude, decoupling of the shedding and vane natural frequencies, minimal impact on downstream rows and performance robustness to manufacturing tolerances. The design assessment[1] indicated that these objectives were achieved in substantial measure.

Given the complexity of the underlying physics of the near/intermediate wake, four different computer codes and turbulence models were used[1] to compute the flow around the baseline and optimized airfoils to assess the reduction in fluctuating amplitude of the surface pressure on the trailing edge of the vane and the impact on the dynamic loads on the downstream rotor. All of the codes solve the RANS equations in conjunction with various turbulence models to provide time-accurate simulations of the flow through the LPOTP turbine. These turbulence models were validated and used effectively for several classes of flows over a period of years prior to the assessment reported in Ref. 1. However, the flow complexities of the very near wake (less than three trailing edge diameters downstream of the blunt trailing edge, see for example Refs. 2 - 4) and limitations of the turbulence models in computing this region of the wake must be kept in mind in evaluating the results presented in Ref. 1. A remarkable finding in Ref. 1 is that all of the codes and corresponding turbulence models indicate essentially the same *qualitative* trends in flow quality and significant performance improvements for the redesigned airfoil. However these RANS simulations were only used to provide a preliminary assessment of the wake characteristics. Numerical simulations that accurately capture the complex physics of wakes and detailed experiments are required to fully understand the wakes of the baseline and optimized airfoils and their interaction with the downstream rows. Among the computational approaches that are available for this exercise, direct numerical simulations are particularly suitable because they do not require any modeling of turbulence and transition. The Reynolds numbers encountered in rotating machinery are typically moderate (less than 2.0×10^6 based on blade chord) and much smaller compared to those found in external flows. Thus simulating the flow in single-stage turbomachinery via DNS on modern supercomputers is possible, albeit computationally expensive.

An excellent overview of transitional and turbulent flow in gas turbine engines can be found in Ref. 5. A description of the different modes of transition that are encountered – natural, bypass, separated flow, periodic unsteady and reverse transition is provided there. Of particular interest is that transition can be multi-modal, that is, multiple modes of transition can co-exist at the same instant in time but in different regions of the airfoil surface. The critical role played by turbulent spots in the transition process and the role of the intermittency function in computing transitional flow properties and its dependency on spot production rate are discussed at length. The effects of freestream turbulence and pressure gradient on spot production rate are also presented here. In Ref. 6 data from extensive testing of multistage axial turbines and compressors are used to obtain an understanding of transition processes in embedded stages.

The effects of Reynolds number, loading, turbulence intensity and frequency of wakes and, clocking of airfoils in alternate rows on the transition process are discussed. Substantial emphasis is placed on defining two relatively distinct periods; one in which transition occurs because of a strong interaction between the wake and the airfoil boundary layer (wake-induced path, predominantly bypass transition) and the other when this is not the case (path between wakes, possible multimodal transition). The paper also discusses the becalmed region behind turbulent spots and strips and the effect of this calming on flow transition and separation. Much of the earlier work in boundary layer transition in turbomachines is reviewed in Refs. 5 & 6.

In a single stage low-speed turbine, interaction effects on the upstream stator are primarily due to the potential flow effect (caused by the relative motion between stator and rotor airfoils). On the other hand the downstream rotor is subjected to wake-blade interaction, interaction between the secondary flows of the stator with the rotor, and as in the case of the stator, the potential flow effect. A true stage simulation that includes both rotors and stators in a single coupled computation is required to better understand the complexities of turbine and compressor flows. Aspects such as the interaction of the secondary flows of upstream rows on downstream airfoils and multi-stage turbomachinery flow physics need a coupled rotor-stator approach. A number of RANS computations of rotor-stator interaction have been reported in the literature. Some of the earlier work is discussed in Refs. 7 - 13 and the references cited therein. Since then there have been a large number of RANS simulations reported and such simulations are used in industry for design as well as assessment. In fact even three-dimensional multistage simulations with the actual number of airfoils in each row are occasionally performed as required. As indicated earlier, although these simulations are configured to include most if not all the geometrical complexity found in turbomachines, and additionally even include cooling flows and aero-elastic effects, they are limited by the adequacy of the transition and turbulence models available today.

MOTIVATION AND OBJECTIVE

Here we provide additional motivation for both using DNS in obtaining the data for assessment of existing or new designs, and, in formal design optimization. The first example is the SSME LPOTP discussed earlier. The data used in this section is from the published literature.

SSME LPOTP First Vane Redesign

The preliminary flow assessments for the baseline and optimized airfoils of Ref. 1 (optimized airfoil is referred to as O5) are presented in this section. The computed data presented here are from Ref. 14. Flow computations were performed using the Baldwin-Lomax turbulence model (one of the models used in Ref. 1). The flow is assumed to be turbulent on both the pressure and suction sides of the airfoil because of the high disturbance levels in the operating environment.

The first redesign of the baseline airfoil (baseline is from the LPOTP of the SSME) is discussed in Ref. 1. The detailed design requirements are also provided there and are outlined below:

- Increase the thickness of the airfoil, particularly in the trailing edge region, to both strengthen the airfoil and increase its natural frequency corresponding to the trailing edge flapping mode
- Reduce trailing edge vortex shedding amplitude
- Decrease trailing edge vortex shedding frequency to obtain greater separation of frequencies (shedding and natural flap mode frequencies)
- Maintain throat area
- Maintain exit flow angle
- Design a trailing edge that eases the manufacturing process (facilitate metal flow in casting)
- Reduce pressure fluctuations on downstream airfoil rows
- Desensitize shedding amplitude to manufacturing tolerances and normal wear and tear

The last requirement was added because the preferred manufacturing technique is casting, with a large manufacturing tolerance of ±0.006 inches (large in relation to the dimensions of the trailing edge).

The baseline airfoil and the optimized airfoil (O5) from Ref. 1 are shown in Fig. 1. Clearly the new airfoil is thicker and stronger. A stress analysis[1] of the baseline and O5 airfoils showed that all relevant measures of stress were lower for O5. The corresponding increase in safety factors for O5 ranged from 3.5 to 6.3. It was concluded in Ref. 1 that the part fitted with the O5 airfoil possessed an essentially infinite life in operation.

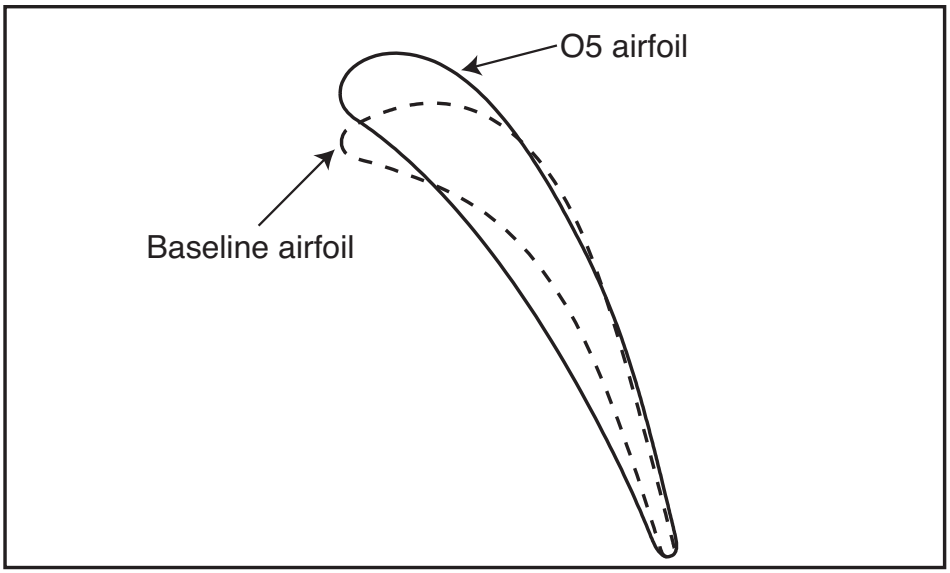

Figure 1. A comparison of the baseline and O5 airfoil shapes, Ref. 14.

Figure 2 shows the computed time-averaged pressure distributions on the baseline and O5 airfoils[14]. Clearly there is a redistribution of the load. The loading on O5 is more uniform. In particular, the loading near the leading edge is higher for O5 than the baseline. Additionally in the last quarter chord, where both the airfoils are leaner, O5 shows a smaller load than the baseline.

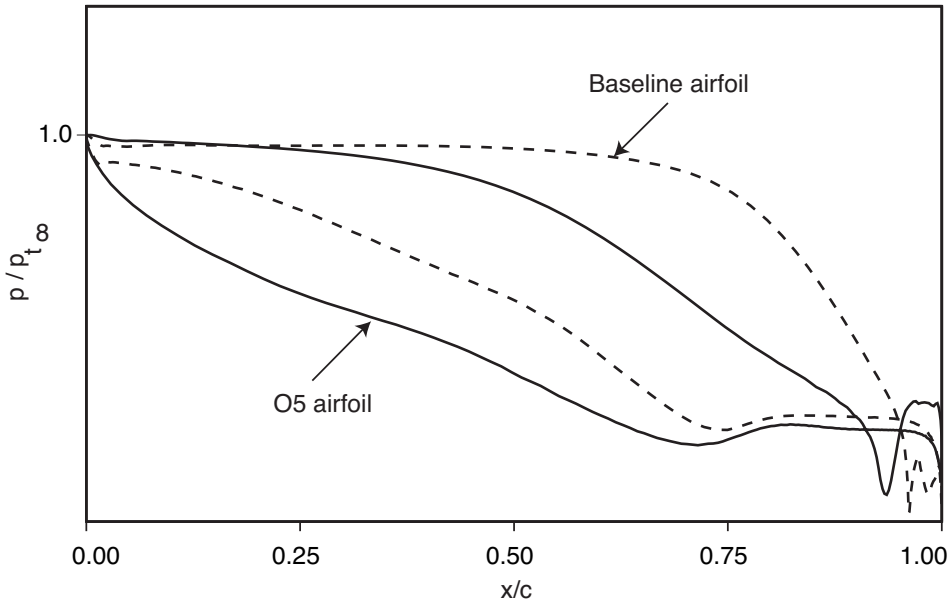

Figure 2. Distribution of the time-averaged surface pressure, Ref. 14.

Figure 3 shows the computed surface pressure amplitudes[14] for the two airfoils (caused by trailing edge vortex shedding). The amplitude distribution obtained with O5 is lower than that obtained with the baseline airfoil on the entire airfoil surface. In particular, O5 shows a reduction of about 75% in peak amplitude (this occurs on the pressure side of the trailing edge).

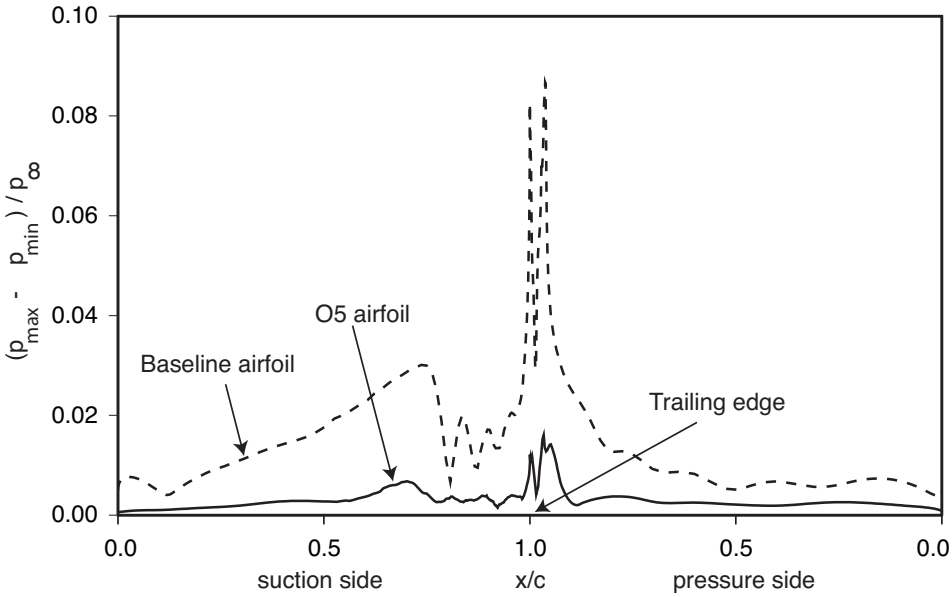

Figure 3. Distribution of the unsteady surface pressure amplitude, baseline and O5 airfoils, Ref. 14.

Figure 4 shows the computed time variation of the surface pressure[14] on O5 and the baseline airfoil at the point of maximum fluctuating pressure amplitude. This point occurs on the pressure side of the trailing edge for both airfoils. The decrease in amplitude

obtained with O5 is clearly visible here. It can also be observed that O5 yields a lower shedding frequency. Figure 5 shows results obtained from a spectral analysis of the waveforms[14] in Fig. 4. Again, the reduction in amplitude obtained with O5 is clearly visible. Additionally, the baseline airfoil sheds at a frequency of 48.6 kilohertz and O5 sheds at 37.8 kilohertz. Thus O5 results in a reduction of approximately 22% in shedding frequency. Based on extensive structural dynamics analyses reported in Ref. 1 it was concluded there that this reduction in shedding frequency coupled with an increase in the flapping mode natural frequency (for O5) results in a detuning of the two frequencies.

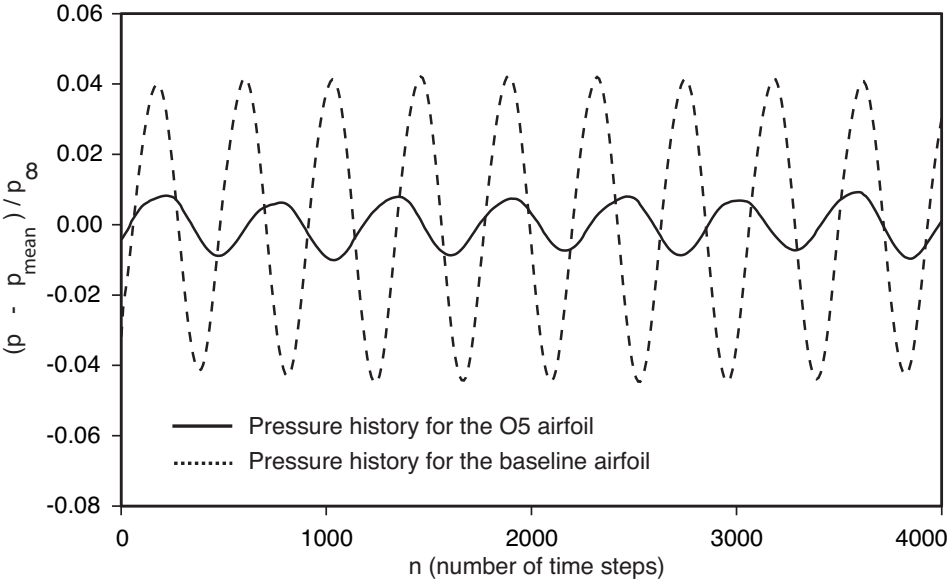

Figure 4. Time-variation of pressure at the point of maximum amplitude, baseline and O5 airfoils, Ref. 14.

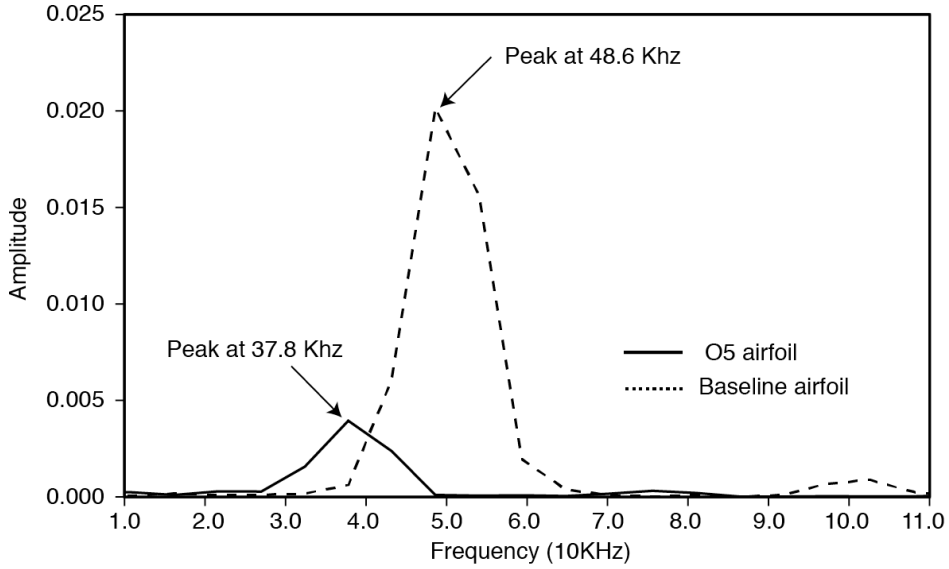

Figure 5. Spectral analysis of the pressure variation at the point of maximum amplitude, Ref. 14.

.

Unsteady rotor-stator computations including the first row of stators (baseline or O5 airfoils), the downstream rotor row and, the second stator row (downstream of the rotor row) are also presented in Ref. 1. These computations show that replacing the baseline airfoils in the first row with the O5 airfoils results in a modest improvement or, no change, in the flow downstream. The results presented in Refs. 1 & 14 demonstrate that the objectives of the optimization effort were achieved to a substantial degree.

However, despite the success indicated in the assessment exercise reported in Refs. 1 & 14, the uncertainty in computing the near/intermediate turbulent wakes with turbulence models remains. How accurately do the models capture the physics of shedding? Are the computed amplitudes and frequencies accurate? Can the computed unsteady pressure values on the trailing edge be trusted? Is the computed intermediate wake represented well enough to result in accurate predictions of unsteady loads on the downstream rotor airfoils? Can the turbulence models be trusted to provide accurate trends of unsteady trailing edge loading on the vane for the perturbations in geometry that are expected (because of the preferred manufacturing technique)? These questions can only be answered by detailed experiments (expensive) or a first-principles approach such as DNS.

Direct numerical simulations of the flow in the first stage of a high-pressure turbine and the flow through a single-stage low-pressure turbine are presented in Refs. 15 - 17. The computed flow features in these investigations exemplify the complexity of the flow in turbine stages and provide additional motivation for including direct numerical simulations in the optimization process. Here we explore the possibility of utilizing DNS in the optimization of turbomachinery airfoil sections.

APPLICATION OF DNS TO DESIGN OPTIMIZATION

A direct numerical simulation is a first-principles approach to computing flow transition and turbulence (model-free). While such simulations are not practical as yet at high Reynolds numbers there are problems of engineering interest, where the Reynolds numbers are modest, that can be solved via DNS. DNS datasets can be used in many ways, the principal ones being a) providing designers with the understanding of the flow necessary for developing advanced designs and flow control mechanisms, b) in the assessment of new designs, c) providing understanding and data necessary for improved turbulence and transition models and d) providing the data for constructing response surfaces or computing optimal search directions in design optimization. The last of these items is probably the most computationally intensive application of DNS. Some in the design/analysis community are of the opinion that given current computing capability, using DNS to generate the aerodynamic data within a formal design optimization process may be impractical. Here we demonstrate, in the case of turbomachinery blading, that there are important design improvements that can be obtained with DNS in the design optimization loop (the related computing costs are discussed in the following section summarizing the effort).

The case in point is the rotor airfoil in the low-pressure turbine (LPT) stage discussed at length in Ref. 17. The performance metric used in the present study is the total pressure loss defined as in Ref. 18 (the difference between the total pressure at the inlet and that at a point 50% axial chord downstream of the trailing edge, divided by the

inlet value). While the loss is defined as a percentage in Ref. 18 it is not in the present study to avoid any confusion with percentage decrease in loss obtained via optimization or percentage differences in loss obtained on fine and baseline grids. The total pressure values used in this definition are obtained via integration in the tangential direction. The Reynolds number based on axial chord and exit flow conditions for the present computation is in the range of 75,000 - 100,000. The inlet Mach number is 0.42 and the average flow-turning angle obtained is 106.7^{o}. All of the computations were performed without freestream turbulence.

Figure 6 shows the computational domain used in the DNS; it is divided into four zones to facilitate grid generation and provide adequate resolution where it is required. The inner "O" grid contains the airfoil. The outer "O" grid interfaces with inner "O" grid and the grids in the inlet and exit regions. The computation is three-dimensional; copies of the two-dimensional zones shown in Fig. 6 are uniformly spaced in the spanwise (z) direction. The grid sizes used in the fine grid computations for assessing the performance of the baseline and optimized airfoils are 2181x91x257 (inner O grid), 999x81x257 (outer O grid), 41x41x257 (inlet grid) and 181x361x257 (exit grid). The total number of grid points utilized for assessment is about 89 million. The extent of the computational domain in the spanwise direction is 0.3C (C is the axial chord) and the wall-normal grid spacing at the airfoil surface is 0.0002C.

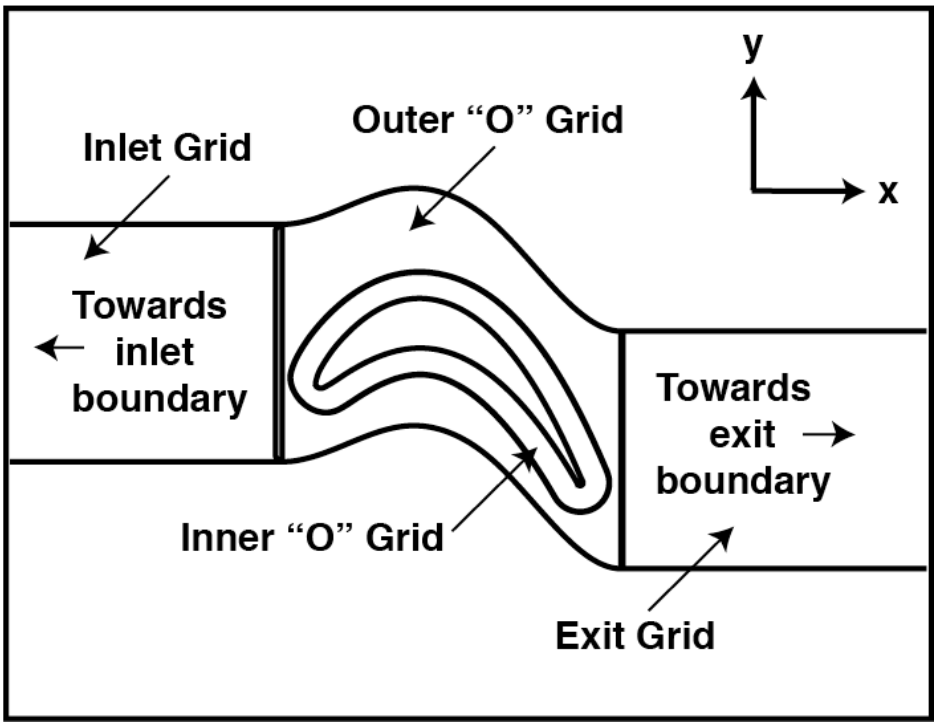

Fig. 6. Airfoil geometry and computational zones used in the direct numerical simulations.

The high-order accurate upwind-biased method developed in Ref. 19 is used here to compute the flow over the airfoils. The inviscid terms are computed using fifth-order accurate upwind-biased finite differences. The viscous terms are computed with fourth-order accurate central differences. The method is iterative-implicit in nature, multiple iterations are used at each time step to solve the nonlinear finite-difference equations

arising from a fully implicit formulation; the method is second-order accurate in time. The boundaries that contain the four computational zones can be broadly classified as natural and zonal boundaries. Both the natural and zonal boundary conditions used in this study are discussed in Ref. 19. Periodic boundary conditions are imposed on the boundaries in the z direction (homogeneity in z). No-slip/adiabatic wall conditions are used on the airfoil surface.

The objective here is to reduce total pressure loss by modifying the shape of the suction surface. The pressure surface is kept unchanged in this first redesign effort. Airfoil parameterization is achieved as in Ref. 20. Total pressure loss was computed via DNS for 7 perturbations of these parameters. A model (response surface) was constructed to represent the variation of loss with varying values of the shape parameters. Details regarding the method of perturbing the parameters and constructing the model are provided in Ref. 21. The search for the optimal airfoil was performed using the model. To reduce computational costs the direct numerical simulations for the perturbed airfoil shapes were performed on a smaller grid than those used for the assessment of the baseline and optimal airfoils (the smaller grid is called the standard grid henceforth). The grid sizes used in these computations for the perturbed geometries are 1401x61x129 (inner O grid), 601x31x129 (outer O grid), 41x41x129 (inlet grid) and 101x181x129 (exit grid). Thus the simulations for the perturbed airfoil shapes used only 16 million grid points each. Standard grid simulations (same grid size as above) were also obtained for the baseline and optimal airfoils and compared with corresponding fine grid simulations in the assessment exercise.

Figure 7a shows the pressure distributions obtained on the standard and fine grids for the baseline airfoil. They are in close proximity even though the fine grid has about 5.5 times as many grid points (with grid refinement in all directions). The total pressure loss obtained on the fine and standard grids for the baseline airfoil differs by only about 6.5%. This comparison of losses and pressure distributions provides us with the necessary confidence to utilize the computed standard grid data in constructing the model, that is, the data are capable of providing the trends in losses with changing airfoil shape (via the model) that are required by the optimizer. A second check wherein the total pressure loss for the baseline airfoil (computed on the standard grid) was compared with the predicted value from the model resulted in a difference of only 3.8% (the baseline airfoil data was not used in obtaining the model). This provides confidence in the ability of the model to accurately predict the losses for various airfoil shapes in the region in design space where the perturbed airfoils reside (assuming the input data is sufficiently accurate), that is, an “inner trust region”. The actual trust region may be substantially larger in extent. If the optimal airfoil resides outside the inner trust region in design space, the associated flow needs to be computed via DNS to ascertain the predicted improvement in performance; here as with the baseline airfoil the computations need to be performed on both the standard and fine grids to demonstrate the adequacy of the computational grids. This final test was performed in the present study.

Figure 7b shows contours of the time-averaged streamwise velocity (u) and the regions of separation on the suction and pressures sides (arrows) obtained for the baseline airfoil on the fine grid. These regions are potential areas of flow quality improvement for the optimization process.

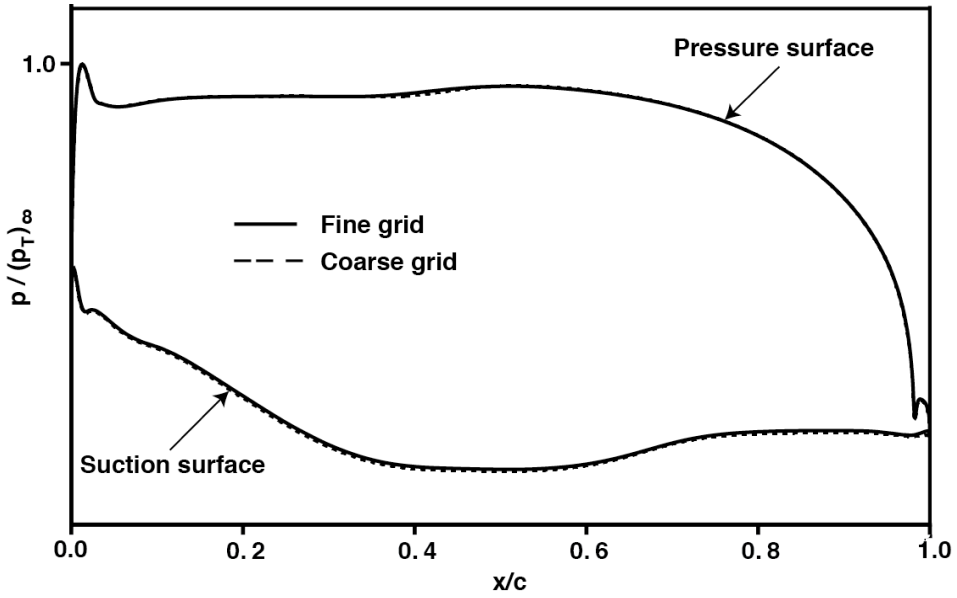

Fig. 7a. Comparison of surface pressure distributions obtained for the baseline airfoil on the standard and fine grids.

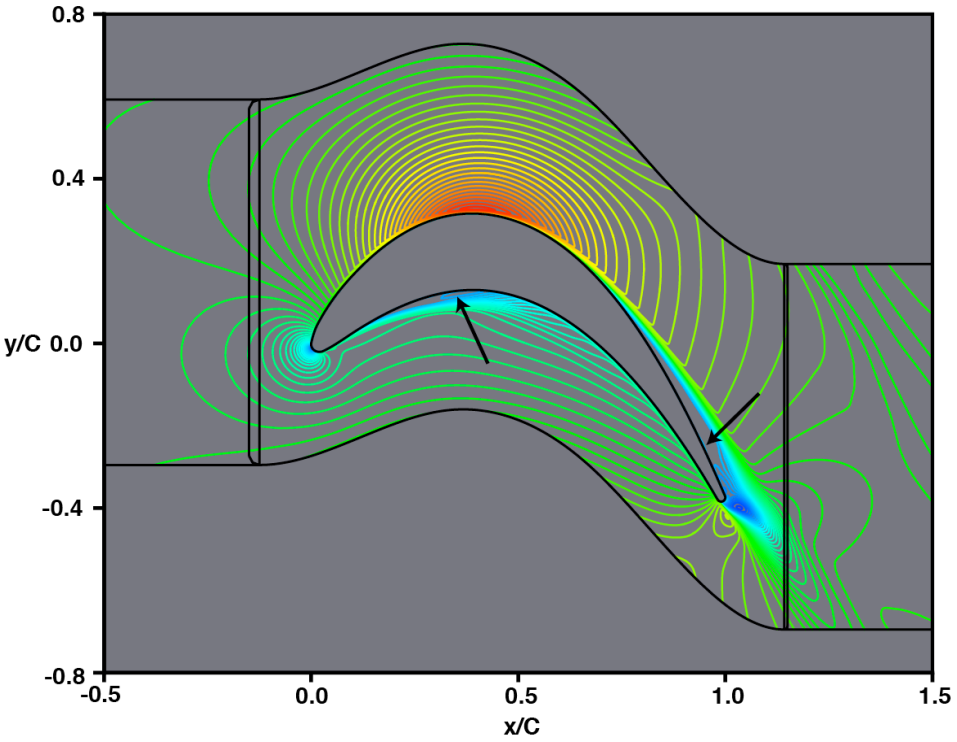

Fig. 7b. Contours of time-averaged streamwise velocity obtained for the baseline airfoil on the fine grid.

As mentioned earlier only the suction side of the airfoil was perturbed and the data from DNSs of the flow associated with the perturbed airfoil sections (total pressure at 50% chord downstream of the trailing edge) were used to construct the model. The pressure surface was left unaltered. The model was used to obtain an airfoil with

improved flow characteristics via a gradient search algorithm (for convenience this first improved airfoil will be referred to as optimal in the rest of this article). Additional DNSs will be required to redesign the pressure surface and also to obtain further refinements to the suction surface of the airfoil obtained with this first model. The flow associated with the airfoil obtained from the optimization process was computed on both the fine and standard grids. The loss coefficients obtained on these two grids differed by only 1.0%. The closer correspondence than that obtained for the baseline airfoil may be because the flow in the case of the optimal airfoil is relatively benign compared to that of the baseline airfoil (this feature will be evident in the figures to follow). The computation performed on the fine grid for the optimized airfoil showed a decrease in total pressure loss of about 43% compared to that obtained on the fine grid for the baseline airfoil. This is a significant improvement in performance. It should be noted however that the present optimization has been carried out at a single specified freestream turbulence level (none), Reynolds number, inlet angle and Mach number. Additional comments regarding airfoil optimization for multiple operating points are provided later in this section.

Figure 8 shows contours of the time-averaged streamwise velocity (u, negative values only) obtained for the baseline airfoil (Fig. 8a) and the optimized airfoil (Fig. 8b) with the fine grid. The minimum and maximum contours levels and the number of contour levels plotted are the same in these two figures.

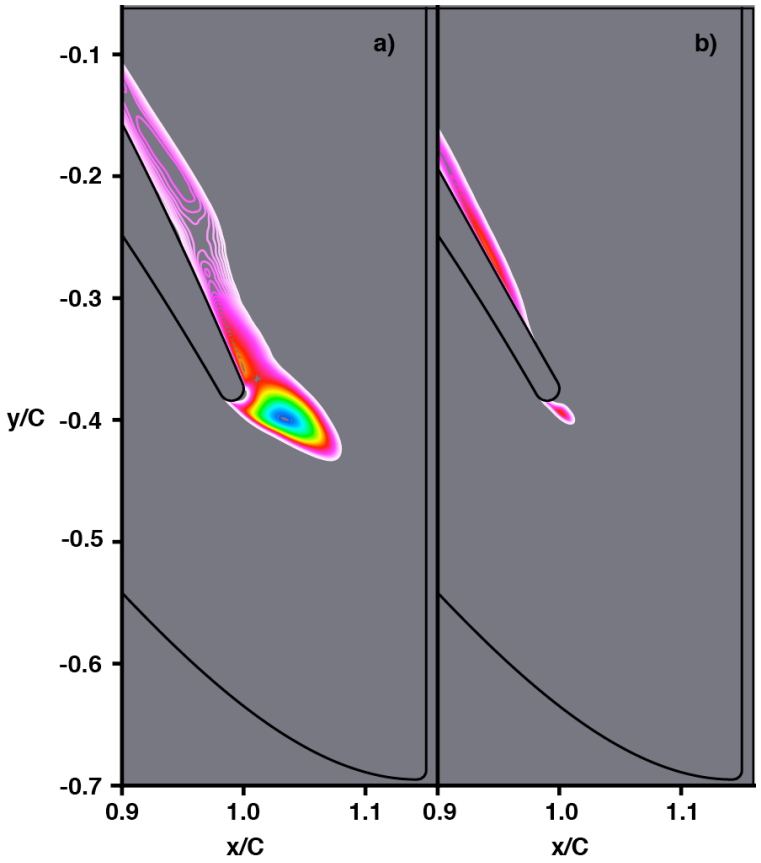

Fig. 8. Contours of time-averaged negative streamwise velocity in the trailing edge region for a) the baseline airfoil and b) the optimized airfoil.

Firstly, the flow is not separated on the suction side of the optimized airfoil very near the trailing edge. The separation bubble is contained on the suction side. This is not the case for the baseline airfoil; the bubble extends beyond the trailing edge and also the peak value of negative u is higher. Secondly, the region of separation above the suction surface is thicker in the case of the baseline airfoil. Clearly optimization has resulted in improved flow quality. The optimized airfoil is more slender in the trailing edge region; the radius of the circular trailing edge is the same in both cases.

Figures 9a and 9b show time-averaged contours of fluctuating kinetic energy for the baseline and optimized airfoils, respectively. As before, the minimum and maximum contour levels and the number of contours are the same in these two figures. The location of the detached shear layer is shown with an arrow in Fig. 9a. Intensity levels increase with increasing x along this shear layer with peak intensities occurring in the near wake region. The optimized airfoil shows peak intensity just above the suction surface and upstream of the trailing region, indicating end-stage transition or early turbulence in the region where the flow reattaches to the suction surface. The peak value itself is lower than that obtained for the baseline airfoil. A comparison of the regions covered by contour lines (wake spread) in Figs. 9a & 9b shows that the wake is thinner for the optimized airfoil. Total pressure profiles in the wake also show the same effect.

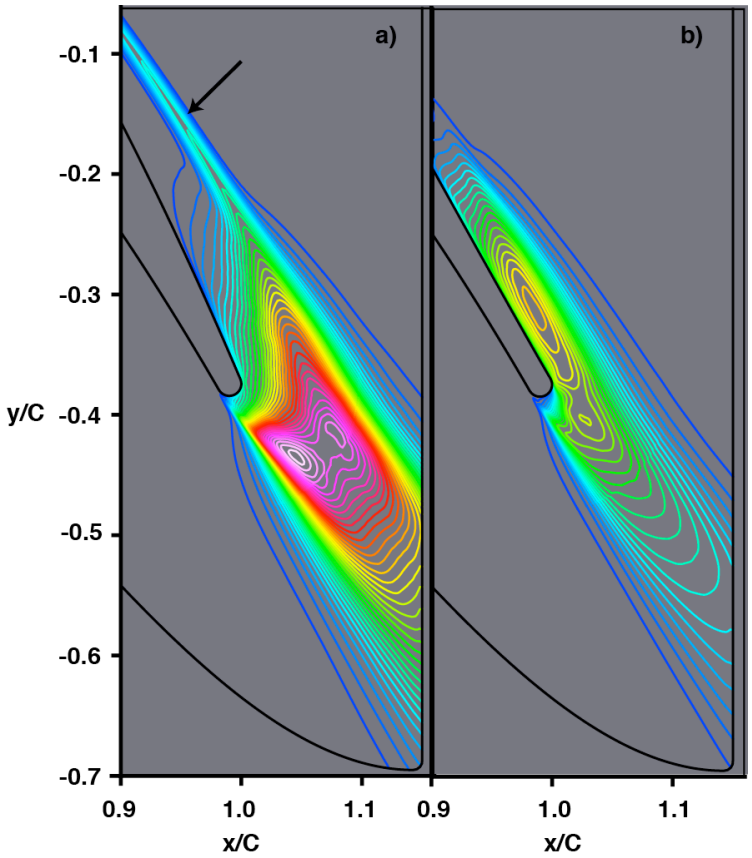

Fig. 9. Contours of time-averaged fluctuating kinetic energy in the trailing edge region for a) the baseline airfoil and b) the optimized airfoil.

It is likely that additional optimization steps that involve perturbing the pressure surface or minor tweaking of the suction surface will yield even better flow quality and lower loss in total pressure. Such an effort will require additional flow simulations and associated response surfaces. However, the emphasis in this exploratory effort is a simple demonstration that it is practical in some cases (with the computing capability currently available) to utilize direct numerical simulations of transitional/turbulent flows at low/moderate Reynolds numbers within an optimization loop to improve aerodynamic design. Efforts to obtain improved performance over a range of Reynolds numbers and different levels of freestream turbulence may result in a multi-objective optimization problem and thus require a suitable optimization method[22]. Designing an airfoil section that is relatively insensitive to operating conditions (for example variations in inlet flow angle) may require the use of concepts such as robust design optimization[22]. Satisfying these additional constraints may require many more direct numerical simulations than used here to obtain the optimal airfoil shape.

CONCLUDING REMARKS

The complexity of turbomachinery flows sometimes precludes the use of RANS codes with their associated transition/turbulence models in achieving specific design objectives and assessing the performance of new designs. Here we explore the use of direct numerical simulations in redesigning a turbine blade section for use in low/moderate Reynolds number flows. The redesign process required seven standard grid simulations (16 million grid points) for constructing a model and two fine grid (89 million grid points) and two standard grid simulations for assessment. The effort yielded an LPT blade section that resulted in improved flow characteristics and a reduction of about 43% in total pressure loss (compared to that obtained for the baseline airfoil). Only the suction surface of the blade was modified in this exploratory effort. It may be possible to further improve flow quality and performance with modifications to the pressure surface of the airfoil and additional minor adjustments to the suction surface.

While the example provided is that of the redesign of a low-pressure turbine blade section with the objective of reducing total pressure loss in a single row, the basic ideas presented here are of course just as applicable elsewhere in aerodynamic shape optimization as long as the computational cost associated with direct numerical simulations is not excessive. The optimization presented here was performed on different computers using different processors. A rough estimate of the total computing time used is 90,000 singe core hours (processors operating at 2.66GHz). The experience gained in this exploratory LPT blade section optimization via DNS suggests that computational costs for the optimization can be significantly reduced in efforts to obtain additional performance improvements.

REFERENCES

1. Marcu, B., Hadid, A., Lin, P., Balcazar, D., Rai, M. M., and Dorney, D. J., “Towards Rocket Engine Components With Increased Strength and Robust Operating Characteristics,” AIAA Paper No. 2005-4449, 41st AIAA/ASME/SAE/ASEE Joint Propulsion Conference, Tucson, Arizona, July 10-13, 2005.

2. Rai, M. M., “Flow physics in the turbulent near wake of a flat plate,” *Journal of Fluid Mechanics*, Volume 724, 2013, pp. 704-733.

3. Rai, M. M., “Flow Phenomena in the very near wake of a flat plate with a circular trailing edge,” *Journal of Fluid Mechanics*, Volume 756, 2014, pp. 510-543.

4. Rai, M. M., “Detached shear-layer instability and entrainment in the wake of a flat plate with turbulent separating boundary layers,” *Journal of Fluid Mechanics*, Volume 774, 2015, pp. 5-36.

5. Mayle, R. E., “The Role of Laminar-Turbulent Transition in Gas Turbine Engines,” Paper No. 91-GT-282, International Gas Turbine and Aeroengine Congress , Orlando, Florida, June 3-6, 1991.

6. Halstead, D. E., Wisler, D. C., Okiishi, T. H., Walker, G. J., Hodson, H. P., Shin, H. W., “Boundary Layer Development in Axial Compressors and Turbines, Part 1: Composite Picture,” Paper No. 95-GT-461, International Gas Turbine and Aeroengine Congress , Houston, Texas, June 5-8, 1995.

7. Rai, M. M., “Navier-Stokes Simulations of Rotor-Stator Interaction Using Patched and Overlaid Grids,” *Journal of Propulsion and Power*, Vol. 3, Sep. – Oct. 1987, pp. 387-396.

8. Rai, M. M., “Three-Dimensional Navier-Stokes Simulations of Turbine Rotor-Stator Interaction; Part 1 – Methodology,” *AIAA Journal of Propulsion and Power*, Vol. 5, No. 3, 1989, pp. 312-319.

9. Rai, M. M., “Three-Dimensional Navier-Stokes Simulations of Turbine Rotor-Stator Interaction; Part 2 – Results,” *AIAA Journal of Propulsion and Power*, Vol. 5, No. 3, 1989, pp. 307-311.

10. Rai, M. M., and Madavan, N. K., “Multi-Airfoil Navier-Stokes Simulations of Turbine Rotor-Stator Interaction,” *Journal of Turbomachinery*, Vol. 112, July 1990, pp. 377-384.

11. Gundy-Burlet, K. L., Rai, M. M., Stauter, R. C., and Dring, R. P., "Temporally and Spatially Resolved Flow in a Two-Stage Axial Compressor. Part II: Computational Assessment." *Journal of Turbomachinery*, Vol. 113, No. 2, April 1991, pp. 227-232.

12. Madavan, N. K., Rai, M. M., and Gavali, S., “Multipassage Three-Dimensional Navier-Stokes Simulation of Turbine Rotor-Stator Interaction,” *AIAA Journal of Propulsion and Power*, Vol. 9, No. 3, 1993, pp. 389-396.

13. Rangwalla, A. A., and Rai, M. M., "A Numerical Analysis of Tonal Acoustics in Rotor-Stator Interactions," *Journal of Fluids and Structures*, Vol. 7, 1993, pp. 611-637.

14. Rai, M. M., “Designing Compact and Robust Rocket Engine Components for Sustainable Space Exploration,” AIAA Paper No. 2006-7098, 11th AIAA/ISSMO Multidisciplinary Analysis and Optimization Conference, Portsmouth, Virginia, September 6-8, 2006.

15. Rai, M. M., "A Direct Numerical Simulation of Transition and Turbulence in a Turbine Stage," AIAA Paper No. 2009-584, 47th AIAA Aerospace Sciences Meeting, January 5-8, 2009, Orlando, Florida.

16. Rai, M. M., "A Direct Numerical Simulation of Turbine Rotor-Stator Interaction," AIAA Paper No. 2009-3685, 39th AIAA Fluid Dynamics Conference, June 22-25, 2009, San Antonio, Texas.

17. Rai, M. M., "A Direct Numerical Simulation of Flow Through a Low Pressure Turbine Stage," AIAA Paper No. 2011-3092, 41st AIAA Fluid Dynamics Conference, June 27-30, Honolulu, Hawaii.

18. Medic, G., and Sharma, O., "Large-Eddy Simulation of Flow in a Low-Pressure turbine Cascade," Paper No. GT2012-68878, Proceeedings of the ASME Turbo Expo 2012: Power for Land, Sea and Air GT2012, June 11-15, 2012, Copenhagen, Denmark.

19. Rai, M. M., "Direct Numerical Simulation of Transitional and Turbulent Flow on a Turbine Airfoil," *AIAA Journal of Propulsion & Power*, Vol. 26, No. 3, 2010, pp. 587-600.

20. Rai, M. M., and Madavan, N. K., "Aerodynamic Design Using Neural Networks," *AIAA Journal*, Vol. 38, No. 1, January 2000, pp. 173-182.

21. Rai, M. M., "A Rapid Aerodynamic Design Procedure Based on Artificial Neural Networks," AIAA Paper No. 2001-0315, AIAA 39th Aerospace Sciences Meeting, January 8 – 11, 2001, Reno, Nevada.

22. Rai, M. M., "Robust Optimal Aerodynamic Design Using Evolutionary Methods and Neural Networks," AIAA Paper No. 2004-778, AIAA 42nd Aerospace Sciences Meeting, January 5 – 8, 2004, Reno, Nevada.